

Strontium-releasing mesoporous bioactive glasses with anti-adhesive zwitterionic surface as advanced biomaterials for bone tissue regeneration

*Original*

Strontium-releasing mesoporous bioactive glasses with anti-adhesive zwitterionic surface as advanced biomaterials for bone tissue regeneration / Pontremoli, Carlotta; Izquierdo-Barba, Isabel; Montalbano, Giorgia; Vallet-Regí, María; VITALE BROVARONE, Chiara; Fiorilli, SONIA LUCIA. - In: JOURNAL OF COLLOID AND INTERFACE SCIENCE. - ISSN 0021-9797. - (2020). [10.1016/j.jcis.2019.12.047]

*Availability:*

This version is available at: 11583/2786666 since: 2020-04-09T16:44:21Z

*Publisher:*

elsevier

*Published*

DOI:10.1016/j.jcis.2019.12.047

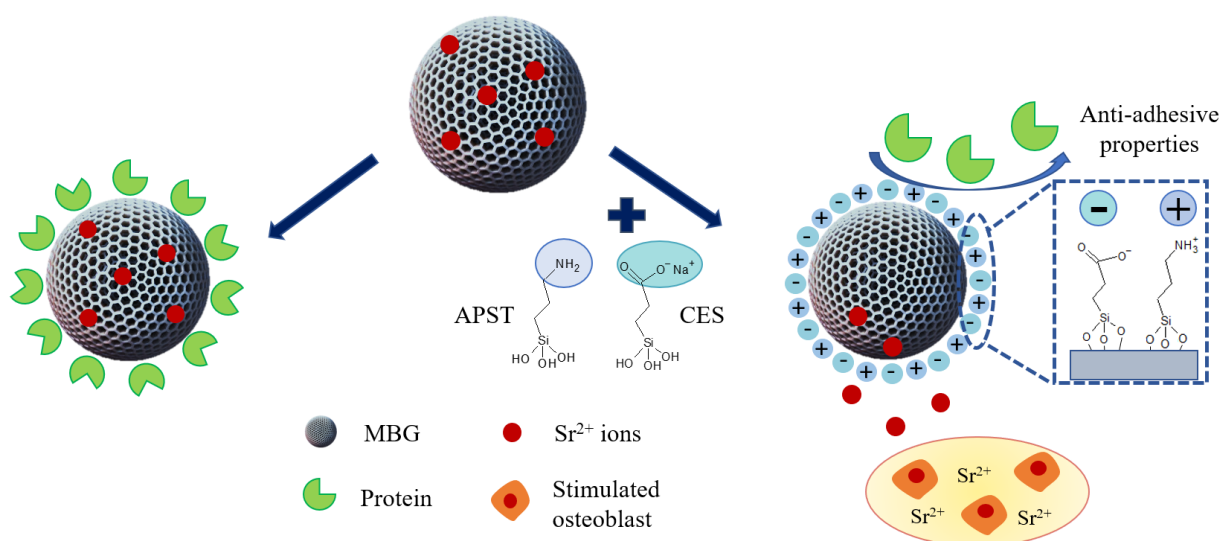
*Terms of use:*

This article is made available under terms and conditions as specified in the corresponding bibliographic description in the repository

*Publisher copyright*

(Article begins on next page)

## Graphical Abstract



## Strontium-releasing mesoporous bioactive glasses with anti-adhesive *zwitterionic* surface as advanced biomaterials for bone tissue regeneration

Carlotta Pontremoli<sup>1</sup>, Isabel Izquierdo-Barba<sup>2,3</sup>, Giorgia Montalbano<sup>1</sup>, María Vallet-Regí<sup>2,3</sup>, Chiara Vitale-Brovarone<sup>1</sup>, Sonia Fiorilli<sup>1\*</sup>

1. Department of Applied Science and Technology, Politecnico di Torino, Corso Duca degli Abruzzi 24, Torino, Italy; carlotta.pontremoli@polito.it (C.P.); giorgia.montalbano@polito.it (G.M.); sonia.fiorilli@polito.it (S.F.); chiara.vitale@polito.it (C.V-B.)

2. Departamento de Química en Ciencias Farmacéuticas, Unidad de Química Inorgánica y Bioinorgánica, Universidad Complutense de Madrid. Instituto de Investigación Sanitaria Hospital 12 de Octubre i+12. Plaza Ramón y Cajal s/n, 28040 Madrid, Spain; : ibarba@ucm.es (I.I.B.); vallet@ucm.es (M.V.R.)

3. CIBER de Bioingeniería, Biomateriales y Nanomedicina, CIBER-BBN, Av. Monforte de Lemos, 3-5, 28029 Madrid, Spain.

\*Correspondence: sonia.fiorilli@polito.it

### Abstract

#### Hypothesis

The treatment of bone fractures still represents a challenging clinical issue when complications due to impaired bone remodelling (i.e. osteoporosis) or infections occur. These clinical needs still require a radical improvement of the existing therapeutic approach through the design of advanced biomaterials combining the ability to promote bone regeneration with anti-fouling/anti-adhesive properties able to minimise unspecific biomolecules adsorption and bacterial adhesion. Strontium-containing mesoporous bioactive glasses (Sr-MBG), which are able to exert a pro-osteogenic effect by releasing  $\text{Sr}^{2+}$  ions, have been successfully functionalised to provide mixed-charge ( $-\text{NH}_3^{\oplus}/-\text{COO}^{\ominus}$ ) surface groups with anti-adhesive abilities.

### *Experiments*

Sr-MBG have been post-synthesis modified by co-grafting hydrolysable short chain silanes containing amino (aminopropylsilanetriol) and carboxylate (carboxyethylsilanetriol) moieties to achieve a *zwitterionic* zero-charge surface. The final system was then characterised in terms of textural-structural properties, bioactivity, cytotoxicity, pro-osteogenic and anti-adhesive capabilities.

### *Findings*

After *zwitterionization* the *in vitro* bioactivity was maintained, as well as the ability to release  $\text{Sr}^{2+}$  ions which are capable of inducing a mineralization process. Irrespective of their size, Sr-MBG particles did not exhibit any cytotoxicity in pre-osteoblastic MC3T3-E1 up to the concentration of 75  $\mu\text{g/mL}$ . Finally, the *zwitterionic* Sr-MBGs showed a significant reduction of serum protein adhesion with respect to the pristine ones. These results open promising future expectations in the design of nanosystems which combine pro-osteogenic and anti-adhesive properties.

## **Keywords**

Mesoporous Bioactive Glasses; Strontium-releasing materials, *zwitterionic* surfaces; pro-osteogenic; anti-adhesive surfaces.

## **1. Introduction**

Under normal healing conditions bony tissue completely regenerates in 6-8 weeks after injuries [1]. Despite this impressive regenerative ability, up to 10–15% of fracture patients still show an impaired healing process, leading to a delayed healing outcome or even to a non-union [2]. Due to the aging population, the total number of patients

suffering from delayed bone healing or non-unions is expected to dramatically increase, since elderly patients have a higher risk of suffering from bone diseases (i.e. osteoporosis) which can result in a compromised healing condition. Despite the promising advancements in the design of novel biomaterials and therapeutic approaches to treat bone fractures and to support bone regeneration in a diseased environment, impaired healing outcomes are still a highly relevant clinical issue [3].

The underlying causes for an unsuccessful healing are various and depend, among others, on the fracture site and severity, patient-dependent factors (e.g., age, chronic or autoimmune diseases) and associated complications, such as the occurrence of bacterial infections. In fact, bone infections remain one of the most potentially devastating impediments for bone healing, with important clinical and socio-economic implications [4–6]. Conventional treatments, based on systemic antibiotic administration [7], implant replacement and surgery [8], can be ineffective and lead to serious complications, causing limitations and a significant reduction of the quality of the patients' lives such as serious side effects [9] and prolonged hospitalization [10]. In this regard, one of the main clinical concerns and causes for the failure of conventional treatments is the evolution and persistence of infections due to the ability of bacteria to form a biofilm [11,12], a microbial community characterized by cells embedded in a matrix of self-produced extracellular polymeric substances [13,14], which allow the bacteria to become resistant to antimicrobial agents [14,15].

To overcome the clinical challenges associated with compromised bone regeneration, a plethora of nano-biomaterials have recently been proposed by the scientific community and used for the development of alternative therapeutic treatments [13–15]. Among the different biomaterials for bone tissue regeneration, mesoporous bioactive glasses (MBGs) are appealing candidates to develop multifunctional biomedical devices, due to their ability to synergistically combine the release of therapeutic ion/drug with anti-fouling/antibacterial properties. In fact, their extremely high exposed surface area and pore volume allow the storage and release of drugs (such as anti-inflammatory or antimicrobial agents) and biomolecules. Moreover, the composition of MBGs can be enriched through the incorporation of specific elements (i.e. Sr, Cu) with the aim of combining in a single biomaterial several therapeutic abilities, such as pro-osteogenic, pro-angiogenic and antibacterial properties. This promising and versatile approach has been previously investigated by the authors [16], who reported the successful incorporation of strontium into an MBG framework and demonstrated, besides the excellent biocompatibility, the pro-osteogenic role of released  $\text{Sr}^{2+}$  ions [16]. Moreover, with the aim of further expanding the therapeutic potential, the co-substitution of different ions

has also been explored [17], by producing Sr-Cu containing MBGs, where the pro-osteogenic effect of strontium was combined with copper which can promote neovascularisation and exert an anti-microbial action [18,19].

Interestingly, the high number of terminal hydroxyl groups allows to easily functionalise MBG surface by grafting alkoxy silane moieties with the aim to achieve several targets, such as greatly improved drug loading ability, the reduction of particle aggregation and nonspecific surface adhesion. In this regard, it is well known that the formation of a nonspecific protein layer on the surface of devices in contact with biological fluids can heavily reduce their performance, due to the inhibitive effect on drug/ion release and on the formation of an apatite layer [20], which is essential for a strong bond with living bone tissue and the promotion of osteogenesis. The adsorption of serum proteins also has a role on the microbial adhesion and biofilm formation [21,22], as the initial attachment of individual bacterial cells or small bacterial aggregates, is usually preceded by the adsorption of biological macromolecules [11,23], such as proteins. For this reason, the design of novel anti-adhesive biomaterials able to prevent bone infections through the inhibition of protein adhesion and, consequently, bacterial attachment and colonisation would represent an attractive and promising strategy.

In this perspective, *zwitterionization* [5] has been extensively exploited and proposed as one of the most promising approaches to design anti-adhesive/anti-fouling surfaces [24,25] with hydrophilic behaviour and electrically neutral charges. *Zwitterionic* surfaces are characterized by an equal number of both positive and negative charges in order to preserve the overall electrical neutrality [26] and the related anti-adhesive properties are imparted by a strongly bonded water molecule layer which acts as a barrier against the adsorption of both proteins and bacteria [5,26]. In fact, the presence of a thick hydration layer allows proteins to preserve a stable conformation when approaching the substrate surface, thus avoiding irreversible adsorption [22,27,28].

Recently, surface *zwitterionization* by means of several functionalization routes has been successfully reported for mesoporous silica nanoparticles to provide them with anti-adhesive properties and enhance their prolonged blood circulation and drug delivery properties [29,30]. Among the explored functionalization strategies, often involving several synthetic steps and potentially toxic by-products [31], the anchoring of low-molecular weight silane moieties carrying functionalities with opposite charge is one of the most promising approach in term of reliability and final clinical translation.

Co-grafting of short chain organosilanes containing mixed charges groups has never been studied and specifically optimised for the surface of substituted-MBG micro- and nanoparticles in view of their application as multifunctional

biomaterials in the field of bone regeneration. To tackle this aim, firstly it is essential to prove that organosilane modification of MBG surface to impart anti-adhesive properties does not hinder or alter substantially the ionic exchange reactions responsible for their intrinsic excellent bioactivity and the release of ions able to exert the desired therapeutic effect (e.g.  $\text{Sr}^{2+}$ ).

With this perspective in this contribution, in order to provide mixed anionic/cationic charges on the surface of the MBGs under physiological conditions ( $\text{pH}=7.4$ ), maintaining a general electrical neutrality, a straightforward and clean methodology based on co-grafting of fully hydrolysable short-chain silane moieties is proposed and fully optimised for Sr-substituted MBGs (Sr-MBG). In particular, Sr-substituted MBGs (Sr-MBG) have been produced in the form of nano- and micro-particles, to obtain materials with different morphological and textural features, and subjected to a co-grafting reaction to introduce almost the same amount of  $-\text{NH}_3^+/-\text{COO}^-$  surface groups, which are expected to impart effective anti-adhesive properties. The functionalisation route based on the post-grafting of aminopropyl silanetriol (APST) and carboxyethylsilanetriol (CES), bearing respectively amino and carboxylate groups, was optimized based on the different reaction kinetics of the two precursors, both in terms of concentration and addition time. Fourier Transform Infrared Spectroscopy (FTIR) analyses highlighted the successful grafting of  $-\text{NH}_3^+/-\text{COO}^-$  groups and  $\zeta$ -potential measurements confirmed the *zwitterionic* nature of the surface as a function of pH.

In order to confirm that the post-functionalization did not inhibit the release property and bioactivity which is typical of unmodified Sr-MBGs, an *in vitro* release of strontium ions was studied in Tris-HCl at pH 7.4 for up to 14 days and *in vitro* bioactivity tests were performed in a simulated body fluid (SBF) to investigate the deposition of an apatite-like layer. *In vitro* biocompatibility assays in the presence of a mouse pre-osteoblastic cell line MC3T3-E1 were also performed to study the effect of post-grafted Sr-MBGs on the osteoblastic cell growth and differentiation. Finally, to assess the anti-adhesive ability imparted by the surface *zwitterionization*, a reduced protein adsorption of serum proteins was evaluated by gel electrophoresis (SDS-PAGE) experiments using bovine serum albumin (BSA) and fibrinogen (Fib), respectively.

## 2. Materials and methods

### 2.1. Zwitterionic Sr-substituted MBGs

Sr-MBGs were prepared through two different synthesis routes to obtain nano- and micro-particles characterised by different textural features in term of exposed specific surface area, pore size and pore volume. The materials were post-functionalized by co-grafting aminopropyl silanetriol (APST) and carboxyethylsilanetriol (CES) as organosilane agents, whose relative amount and reaction time were properly adjusted to reach an almost neutral overall surface charge.

#### *2.1.1. Sr-substituted MBG nanoparticles*

Sr-MBGs nanoparticles have been prepared by using a base-catalysed sol-gel synthesis, following the procedure reported previously by the authors[16]. In particular, MBGs with 2% molar percentage of Sr (molar ratio Sr/Ca/Si = 2/13/85, named hereafter as MBG\_Sr2%\_SG) was prepared as follows: 6.6 g cetyltrimethylammonium bromide (CTAB  $\geq 98\%$ , Sigma Aldrich, Italy) and 12 mL  $\text{NH}_4\text{OH}$  (Ammonium hydroxide solution, Sigma Aldrich, Italy) were dissolved in 600 mL of double distilled water ( $\text{ddH}_2\text{O}$ ) under stirring for 30 min. Then, 30 mL tetraethyl orthosilicate (TEOS, Tetraethyl orthosilicate, reagent grade 98%, Sigma Aldrich, Italy), 4.888 g of calcium nitrate tetrahydrate ( $\text{Ca}(\text{NO}_3)_2 \cdot 4\text{H}_2\text{O}$ , 99%, Sigma Aldrich, Italy) and 0.428 g of strontium chloride ( $\text{SrCl}_2$  99%, Sigma Aldrich, Italy) were added under vigorous stirring for 3 h. The powder was collected by centrifugation (Hermle Labortechnik Z326) at 11,000 rpm for 5 min, washed one time with distilled water and two times with absolute ethanol. The final precipitate was dried at 70 °C for 12 h and calcined at 600 °C in air for 5 h at a heating rate of 1 °C  $\text{min}^{-1}$  using a Carbolite 1300 CWF 15/5, in order to remove CTAB.

All the reagents were purchased from Sigma Aldrich, Italy and used as received.

#### *2.1.2. Sr-substituted MBG microparticles*

Sr-MBGs in the form of microspheres with 2% molar percentage of Sr (molar ratio Sr/Ca/Si = 2/13/85, hereafter named as MBG\_Sr2%\_SD) were produce by using a spray-drying method, based on a modification of the procedure reported by Pontiroli et al. [32]. Briefly, 2.030 g of the non-ionic block copolymer Pluronic P123 ( $\text{EO}_{20}\text{PO}_{70}\text{EO}_{20}$ , average  $M_n \sim 5,800$ , Sigma Aldrich, Italy) were dissolved in 85 g of  $\text{ddH}_2\text{O}$ . In a separate batch, a solution of 10.73 g of TEOS was pre-hydrolysed under acidic conditions using 5 g of an aqueous HCl solution at pH 2 until a transparent solution was obtained. The solution with TEOS was then added drop by drop into the template solution and kept stirring for 30 min. Then, 0.163 g of strontium chloride and 1.86 g of calcium nitrate tetrahydrate were added and the final solution was stirred for 15 min and then sprayed (Büchi, Mini Spray-Dryer B-290) using nitrogen as the atomizing gas with the following parameters: inlet temperature 220 °C,  $\text{N}_2$  pressure 60 mmHg and feed rate 5

mL/min. The obtained powder was collected and calcined at 600 °C in air for 5 h at a heating rate of 1 °C min<sup>-1</sup> using a Carbolite 1300 CWF 15/5.

All the reagents were purchased from Sigma Aldrich, Italy and used as received.

### 2.1.3. Zwitterionic Sr-MBGs

To provide *zwitterionic* properties, Sr-MBGs were post-grafted with 3-aminopropylsilanetriol (APST) (22-25% in water, ALFA Chemistry) and carboxyethylsilanetriol sodium salt (CES, 25% vol. in water, Carbosynth Limited). In particular, 0.5 g of dried powder were first outgassed overnight in vacuum and then dispersed in 100 mL of absolute ethanol (Ethanol puriss. P.A., absolute = 99.8%, Sigma Aldrich, Italy). The initial amount of APTS and CES to be added to the suspension was calculated referring to the Zhuravlev number [33], which is widely used in the literature for the estimation of the organosilane precursors in post-grafting reactions of mesoporous silicas and MBGs. Indeed, according to the Zhuravlev number, a density 4.9 SiOH/nm<sup>2</sup> can be considered, and based on the measured specific surface area of MBGs, the overall number of exposed hydroxyls (acting as anchoring sites for grafting) was estimated and the amount of precursors derived accordingly. The optimisation of the overall procedure was not entirely straightforward and required several step-by-step adjustments. To this aim,  $\zeta$ -potential measurements were conducted as preliminary evaluation of the modification of surface charge imparted by grafting, in order to guide the corrections required to reach the *zwitterionic* behaviour.

At first, an equimolar concentration of APST and CES (0.3 mmol) was added simultaneously to the ethanol suspension and refluxed 24 h under stirring (200 rpm) at 80 °C under nitrogen atmosphere. The resulting functionalized powders were filtered, washed three times with absolute ethanol and dried overnight at 70°C.

As reported in table 1 (first row),  $\zeta$ -potential measurements at pH 7.4 revealed a negative value (-9 mV), suggesting higher surface reactivity for CES compared to APST. Therefore, to increase the amount of surface positive charges, a double amount of APST (0.6 mmol) was added to the ethanol solution and kept stirring for 30 min prior the addition of CES (0.3 mmol), in order to allow the reaction between MBG surface and APST. Lastly, an amount of APST equal to 0.9 mmol (molar ratio APST:CES 3:1) resulted to be the most appropriate to reach an overall surface charge close to zero, as shown by table 1 (third row). The samples reacted with APST:CES 3:1 molar ratio will be referred hereafter as MBG\_Sr2%\_SG\_Z and MBG\_Sr2%\_SD\_Z and were selected for the physico-chemical characterization and for the biological assessment. Fig. 1 displays functionalization procedure to obtain the *zwitterionic* materials.



Table 1 Investigated APST/CES amounts (mmol) and addition time. Zeta potential values measured at pH 7.4 of the resulting functionalized MBG\_Sr2%.

| mmol APST | mmol CES | Addition time          | $\zeta$ -potential pH 7.4 |
|-----------|----------|------------------------|---------------------------|
| 0.3       | 0.3      | Simultaneously         | -9 mV                     |
| 0.6       | 0.3      | CES added after 30 min | -7 mV                     |
| 0.9       | 0.3      | CES added after 30 min | -2 mV                     |

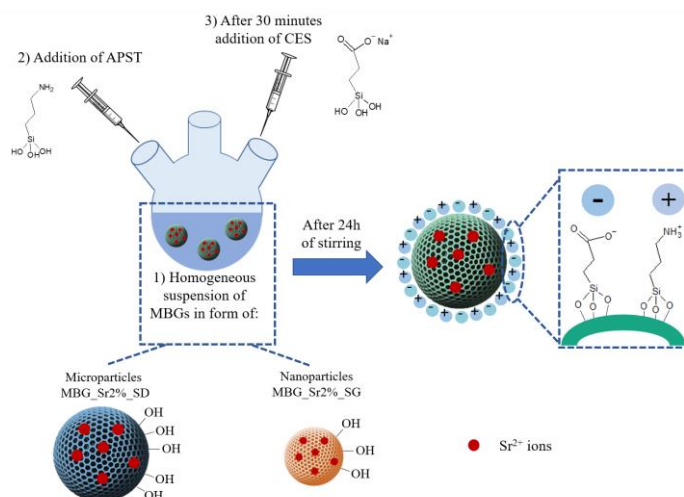


Fig. 1 Functionalization procedure to obtain zwitterionic Sr-MBGs.

## 2.2. Physico-chemical characterization

The mesoporous structure of materials was characterised by low angle X-ray diffraction (XRD) and transmission electron microscopy (TEM). XRD experiments were performed on a Philips X'Pert diffractometer equipped with a Cu K $\alpha$  (40 kV, 20 mA) source over the range 0.6–8.0  $\theta$ , with a step of 0.02  $\theta$  and a contact time of 5 s. TEM images were recorded in a JEOL 3010 electron microscope (JEOL, Japan) operating at 300 keV coefficient of objective lens (Cs) equal to 0.6 mm, resolution 1.7 Å, employing a CCD camera (1024 x 1024 pixels, size 24 x 24 lm; MultiScan model 794, Gatan, UK) under low dose conditions.

The morphology of the produced particles was analysed by Field-Emission Scanning Electron Microscopy (FE-SEM) using a ZEISS MERLIN instrument. For FE-SEM observations, 10 mg of MBG\_Sr2%\_SG\_Z were dispersed in 10 mL of isopropanol using an ultrasonic bath (Digitec DT 103H, Bandelin) for 5 min to obtain a stable suspension. The resulting suspension was dropped on a copper grid (3.05 mm Diam.200 MESH, TAAB), allowed to dry and successively chromium-coated prior to imaging (Cr layer of *ca* 7 nm). At variance, MBG\_Sr2%\_SD\_Z powder was dispersed directly to a conductive carbon tape adhered on a stub and coated with the Cr layer (7 nm).

Textural properties were analysed by N<sub>2</sub> adsorption-desorption measurement conducted by ASAP2020, Micromeritics analyser at a temperature of −196 °C and before measurements, samples were outgassed at 150 °C for 5 h. The Brunauer-Emmett-Teller (BET) equation was used to calculate the specific surface area (SSA<sub>BET</sub>) from the adsorption isotherm in the 0.04–0.2 relative pressure range. The mesoporous silica pore size distribution was calculated through the DFT method (Density Functional Theory) using the NLDFT kernel of equilibrium isotherms (desorption branch).

The successful anchoring of functional groups was assessed by Fourier Transform infrared spectroscopy (FT-IR), thermo-gravimetric analysis (TGA) and  $\zeta$  potential measurements. FT-IR spectra were collected using a FT-IR spectrometer (Bruker Equinox 55 spectrometer) in the 4000–400 cm<sup>−1</sup> wavenumber range. TGA were conducted on a TG 209 F1 Libra instrument (Netzsch) over a temperature range of 25–600 °C with a heating rate of 10 °C/min under air in a flow of 50 mL/min).

$\zeta$ -potential measurements (Zetasizer nano ZS90 Malvern Instruments Ltd.) were conducted in aqueous media at different pH values in order to determine in which pH range the material surface preserves *zwitterionic* nature, i.e. the isoelectric point, which is closely related to the zero point charge [34]. The experiment was performed three times for each sample and data are presented as means  $\pm$  standard deviations.

### 2.3. *In vitro* bioactivity of *zwitterionic* MBGs

*In vitro* bioactivity test was performed in simulated body fluid (SBF), according to the protocol described in the literature [35], with the aim to evaluate the apatite-forming ability of the functionalized Sr-substituted MBGs. To this aim, 30 mg of Sr-MBGs were soaked in 30 mL of SBF at 37 °C up to 14 days in an orbital shaker (Excella E24, Eppendorf, Milan, Italy) with an agitation rate of 150 rpm. At each time point (3 h, 1 day, 3 days, 7 days and 14 days), the suspension was centrifuged at 10,000 rpm for 5 min, the collected powder was washed twice with distilled water and dried in oven at 70 °C for 12 h prior FE-SEM and XRD analysis to evaluate the apatite layer formation. Moreover, the pH of each recovered supernatant was measured, to assess if the values are suitable for allowing osteoblasts to maintain their physiological activity [36].

### 2.4. *Sr*<sup>2+</sup> release from *zwitterionic* MBGs

The concentration of Sr<sup>2+</sup> ions released from *zwitterionic* MBGs was evaluated by soaking the powders in Tris HCl buffer (Tris(hydroxymethyl)aminomethane (Trizma) (Sigma Aldrich, Milan, Italy) 0.1 M, pH 7.4) at concentration of 250  $\mu$ g/mL [16,19]. In particular, 5 mg of powder were suspended in 20 mL of buffer up to 14 days at 37 °C in an

orbital shaker (Excella E24, Eppendorf) with an agitation rate of 150 rpm. At defined time points (3 h, 24 h, 3 days, 7 days and 14 days) the suspension was centrifuged at 10,000 rpm for 5 min (Hermle Labortechnik Z326, Wehingen, Germany), half of the supernatant was collected and replaced by the same volume of fresh buffer solution to keep constant the volume of the release medium. The release experiments were carried out in triplicate. The concentration of  $\text{Sr}^{2+}$  ions was measured by Inductively Coupled Plasma Atomic Emission Spectrometry Technique (ICP-AES) (ICP-MS, Thermoscientific, Waltham, MA, USA, ICAP Q), after appropriate dilutions. To evaluate the effective amount of strontium incorporated into MBGs during the synthesis, the powders were dissolved in a mixture of nitric and hydrofluoric acids (0.5 mL of  $\text{HNO}_3$  and 2 mL of HF for 10 mg of powder) and the resulting solutions were measured via ICP analysis. The experiment was performed three times for each sample and data are presented as means  $\pm$  standard deviations.

## 2.5. Biological assessment

### 2.5.1. *In vitro* biocompatibility tests

Cell culture experiments were performed using the mouse MC3T3-E1 osteoblast cell line, plated at an initial density of 10,000 cells  $\text{cm}^{-2}$  in a multi-well plates and incubated in 2 mL of Dulbecco's modified Eagle's medium (DMEM) (Sigma Chemical Co., St. Louis, USA) supplemented with 10% heat-inactivated fetal bovine serum (FBS) (Lonza BioWhittaker, Spain), 1 mM L-glutamine (Lonza BioWhittaker, Spain), 200  $\mu\text{g mL}^{-1}$  penicillin (Lonza BioWhittaker, Spain) and 200  $\mu\text{g mL}^{-1}$  streptomycin (Lonza BioWhittaker, Spain) at 37°C in 5%  $\text{CO}_2$ .

Sr-substituted MBGs (before and after functionalisation) were suspended at different concentrations (25, 50 and 75  $\mu\text{g/mL}$ ) in completed DMEM, sonicated in order to obtain a stable suspension and placed into each 24-well plates after cell seeding. Wells without MBG particles were used as control.

Three different measurements of two independent experiment were performed in order to determine the statistical analyses.

### 2.5.2. Mitochondrial activity – MTT

Cell proliferation induced by both unmodified and *zwitterionic* Sr-substituted MBGs was determined by MTT test. MC3T3-E1 cells were seeded for 24 h as previously described and then incubated at 37°C in 5%  $\text{CO}_2$  with different particle concentrations (25, 50 and 75  $\mu\text{g/mL}$ ) for different time periods (1 day, 2 days and 5 days). At each time point, 300  $\mu\text{L}$  of CellTiter 96® AQueous One Solution Reagent (containing 3-(4,5-dimethylthiazol-2-yl)-5-(3-

carboxymethoxyphenyl)-2-(4-sulfophenyl)-2H-tetrazolium salt (MTS) and an electron coupling reagent (phenazine ethosulfate) that combines with MTS to form a stable solution) was added to each well and incubated for 2 h. then, 100  $\mu$ l of each cell conditioned medium was placed in a 96-well plate and the absorbance at 490 nm was measured in an Opsys MR Reader (Dynex Technologies, Chantilly, VA, USA).

#### *2.5.3. Cytotoxicity test –Lactate dehydrogenase (LDH) measurement*

Biocompatibility and cytotoxic effects of unmodified and *zwitterionic* Sr-substituted MBGs were tested measuring the amount of released cytosolic lactate dehydrogenase (LDH) enzyme caused by the cellular membrane damage (Spinreact S.A., Spain). The assay is based on the reduction of NAD by LDH. The resulting reduced NAD (NADH) is exploited in the stoichiometric conversion of a tetrazolium dye.

The supernatants of particles-cells incubation experiments were collected after 1 day of incubation and mixed with the LDH kit reagents (SPINREACT®, imidazole 65 mmol/L, pyruvate 0.6 mmol/L and NADH 0.18 mmol/L). The absorbance of the resulting coloured compound was measured at 340 nm wavelength at 0, 1, 2, and 3 min, calculating the amount of enzyme that transforms 1 mmol of substrate per minute in standard conditions (U/L) as  $\Delta A/\text{min} \times 4925$  (where  $\Delta A$  is the average difference per minute and 4925 corresponds to the correction factor for 25–30 °C).

#### *2.5.4. Mineralization assay*

Matrix mineralization was measured in MC3T3-E1 cell cultures by alizarin red staining, as described in the protocol reported by Lozano et al. [37]. After incubation with the tested materials for 15 days, cells were washed three times with PBS and then fixed with 75% ethanol for 1 h. Cell cultures were stained with 40 mM alizarin red in distilled water (pH 4.2) for 10 min at room temperature. Subsequently, cell monolayers were washed five times with distilled water and the stain was dissolved with 10% cetylpyridinium chloride in 10 mM sodium phosphate, pH 7, measuring absorbance at 620 nm.

#### *2.6. Anti-adhesive abilities assessment: serum protein adhesion assay*

*In vitro* adhesion of proteins was determined using bovine serum albumin (96% BSA, A2153 Sigma-Aldrich) and fibrinogen (75% Fib, F8630 Sigma-Aldrich). A 50% v/v solution of such proteins (2 mg/mL for BSA and Fib in PBS 1x, respectively) was gently mixed with both unmodified and *zwitterionic* Sr-MBGs (2 mg/mL in PBS 1x) and kept under orbital agitation (200 rpm) during 24h at 37 °C. Particle suspensions were then centrifuged (10,000 rpm) and washed with fresh PBS to eliminate free or loosely bound proteins and a one-dimensional sodium dodecyl sulfate-polyacrylamide gel electrophoresis gel (SDS-PAGE) assay was performed. Briefly, the recovered supernatants were

mixed with a buffer (Tris 6 mM, SDS 2%, glycerol 10%, 2- $\beta$ -mercaptoethanol 0.5 M, traces of bromophenol blue, pH = 6.8) and loaded in 10% SDS-PAGE gels. A calibration curve was estimated by loading 0.5, 1.0, 1.5, 2.0 and 2.5  $\mu$ g/mL protein concentrations. The gels were run with a constant 100 V voltage (45-60 min) and stained in R-250 colloidal Coomassie blue solution for visualization. Imagen J software was used in order to determine the amount of adsorbed proteins through calibrated line of the different proteins. Three different measurements of two independent experiment were performed in order to determine the statistical analyses.

The anti-adhesive ability of the bare and *zwitterionic* Sr-MBGs nanoparticles prepared by SG approach was also evaluated using dynamic light scattering (DLS) method. The size distribution was measured on a Zetasizer nano ZS90 (Malvern Instruments Ltd.) before and after powder incubation in the BSA solution for 24 h. In particular, samples at a concentration of 1 mg/mL were soaked in a 1 mg/mL BSA solution in PBS and kept under stirring (300 rpm) for 24h at 37 °C. The suspensions were then centrifuged, the collected powders were washed with ddH<sub>2</sub>O and re-suspended in PBS for the measurement. The mean value of three different experiments was used as hydrodynamic diameter (Dh).

### 3. Results and discussion

#### 3.1. Physico-chemical characterization

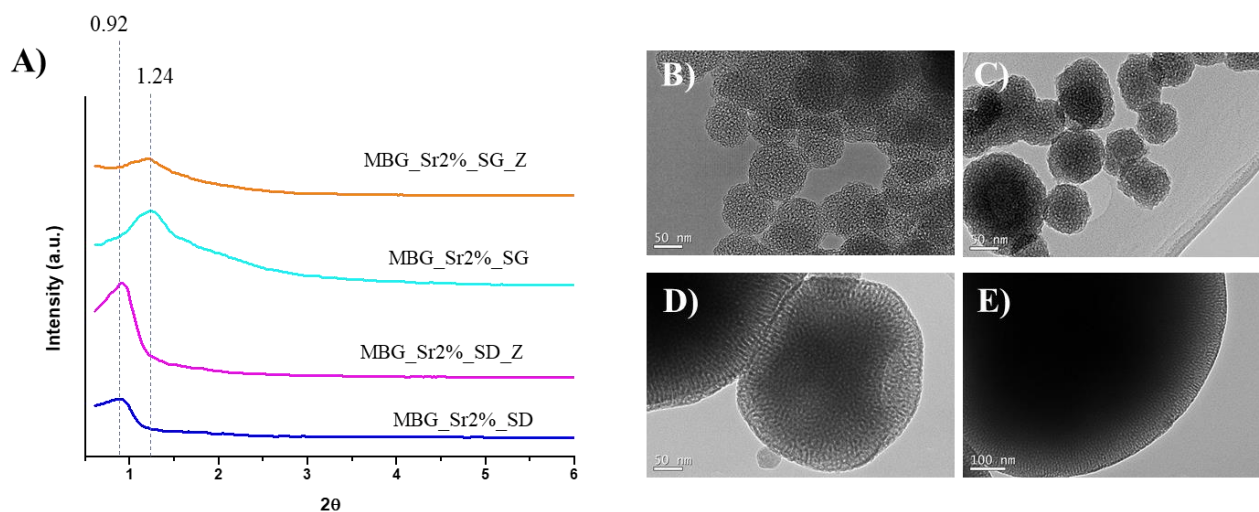


Fig. 2 (A) Low-angle XRD of unmodified and *zwitterionic* Sr-MBGs. TEM images of: (B) MBG\_Sr2%\_SG; (C) MBG\_Sr2%\_SG\_Z; (D) MBG\_Sr2%\_SD; (E) MBG\_Sr2%\_SD\_Z.

The mesostructure of unmodified and *zwitterionic* Sr-MBGs has been evaluated by TEM and low-angle XRD (Fig 2). TEM images evidenced a worm-like mesoporosity throughout both nanoparticles (Fig 2.B) and microparticles,

respectively (Fig 2.D), also clearly discernible after the functionalization (Fig 2.C-E). Low-angle XRD patterns (Fig 2.A) confirm the worm-like porous structure [30,38,39], in fact both MBG\_Sr2%\_SG and MBG\_Sr2%\_SD, before and after functionalization, showed a single peak, respectively at around  $1.24^{\circ}$  and  $0.92^{\circ}$ , corresponding to the (100) reflection. The decrease of the reflection intensity revealed upon silane co-grafting can be ascribed to a limited and confined collapse of the mesoporous structure.

Morphological analysis of MBG\_Sr2%\_SG\_Z showed particles with uniform spherical shape and size ranging between 100 and 200 nm, while MBG\_Sr2%\_SD\_Z, revealed spherical particles with micrometric size between 0.5 and 5  $\mu\text{m}$  (Fig SI 1). These results resulted in good agreement with morphology, size and shape revealed by the observation of unmodified analogues materials[16], evidencing that the post-synthesis modification did not significantly alter the morphological features of Sr-MBGs.

ICP-AES analysis conducted on acid-digested powder revealed that only 30% of strontium precursor was effectively incorporated for MBG\_Sr2%\_SG, at variance with MBG\_Sr2%\_SD samples whose incorporated strontium amount resulted very similar to the theoretical value. ICP analysis on samples after the post-synthesis reaction evidenced that incorporated strontium amount resulted unaffected, demonstrating that the functionalization reaction did not induce any loss of incorporated strontium amount.

The textural features of the samples before and after functionalization were investigated by  $\text{N}_2$  adsorption/desorption measurements. MBG\_Sr2%\_SG showed a type IV isotherm, characteristic of mesoporous materials and a pore size distribution centred at around 4.2 nm (Fig 3.A-B).

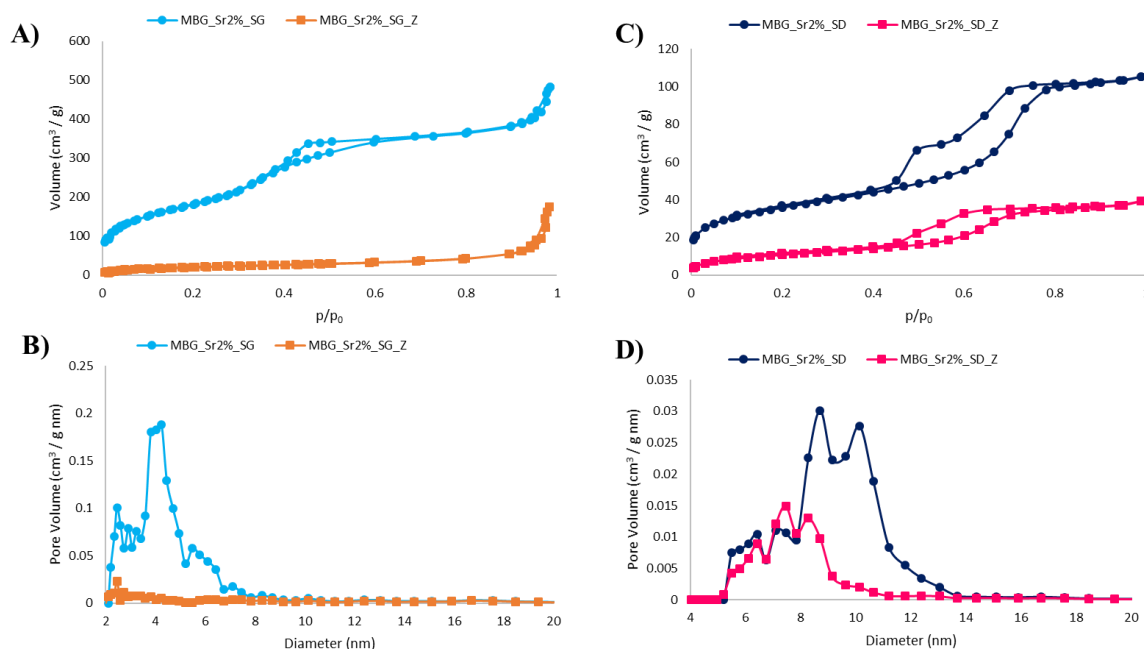


Fig. 3 N<sub>2</sub> adsorption-desorption isotherm of MBG\_Sr2%\_SG and MBG\_Sr2%\_SG\_Z (A), MBG\_Sr2%\_SD and MBG\_Sr2%\_SD\_Z (C). DFT pore size distribution of MBG\_Sr2%\_SG and MBG\_Sr2%\_SG\_Z (B), MBG\_Sr2%\_SD and MBG\_Sr2%\_SD\_Z (D).

The material exhibits excellent textural properties, in terms of very high surface area (670 m<sup>2</sup> g<sup>-1</sup>) and pore volume (0.63 cm<sup>3</sup> g<sup>-1</sup>), as reported in Table 2. After the functionalization, a modification of the isotherm and a drastic decrease in SSA and pore volume (Table 2) is observed, suggesting that mesopore entrances are partially or even fully blocked by the organosilane grafting [30,40]. In fact, if the organosilanes react at the pore entrances during the initial phases of reaction, the diffusion of precursors within the mesopore can be compromised, leading to an uneven distribution and, in some cases, to the almost closure of the pores [40].

N<sub>2</sub> adsorption-desorption isotherm of MBG\_Sr2%\_SD is a IV type isotherm with a pronounced hysteresis loop. The related values of specific surface area SSA, pore volume and pore size are reported in table 2 and are in accordance to those previously obtained for analogue systems [16]. As expected after grafting, MBG\_Sr2%\_SD\_Z exhibits lower specific surface area and pore volume and size compared with unmodified sample, but at variance with MBG\_Sr2%\_SG\_Z, a noticeable residual surface area and pore volume is retained after silane anchoring, evidencing that pores do not undergo complete occlusion but experienced a size reduction (from 8-11 nm to 6-9 nm).

Table 2 Textural parameters of MBG\_Sr2%\_SG, MBG\_Sr2%\_SG\_Z, MBG\_Sr2%\_SD and MBG\_Sr2%\_SD\_Z.

| MBG_Sr2%_SG | MBG_Sr2%_SG_Z | MBG_Sr2%_SD | MBG_Sr2%_SD_Z |
|-------------|---------------|-------------|---------------|
|-------------|---------------|-------------|---------------|

|                          |                                      |                                      |                                      |                                      |
|--------------------------|--------------------------------------|--------------------------------------|--------------------------------------|--------------------------------------|
| <b>BET surface area</b>  | 670 m <sup>2</sup> g <sup>-1</sup>   | 76 m <sup>2</sup> g <sup>-1</sup>    | 126 m <sup>2</sup> g <sup>-1</sup>   | 40 m <sup>2</sup> g <sup>-1</sup>    |
| <b>Average Pore size</b> | 4.2 nm                               | -                                    | 8-11 nm                              | 6-9 nm                               |
| <b>Pore volume</b>       | 0.63 cm <sup>3</sup> g <sup>-1</sup> | 0.16 cm <sup>3</sup> g <sup>-1</sup> | 0.16 cm <sup>3</sup> g <sup>-1</sup> | 0.06 cm <sup>3</sup> g <sup>-1</sup> |

FT-IR spectroscopy allowed to assess the successful anchoring of functional groups. Figure 4 shows the FT-IR spectra of both bare and *zwitterionic* samples. All spectra display in the range of 3750–3000 cm<sup>-1</sup> the typical absorption bands, corresponding to the stretching vibrational frequencies of the H-bonded hydroxyls. The spectra of functionalized samples show significant changes compared to the bare analogues, in particular, two bands at 1550 and 1407 cm<sup>-1</sup>, ascribed respectively to the asymmetric ( $\nu_{as}$ ) and symmetric ( $\nu_s$ ) stretching vibration of the carboxylate group COO<sup>-</sup> [41], and two shoulders at around 1650 cm<sup>-1</sup> and 1520 cm<sup>-1</sup> corresponding to the bending mode of protonated amine group NH<sub>3</sub><sup>+</sup> [42]. On contrary, the C=O adsorption band of protonated COOH group, displayed at 1706 cm<sup>-1</sup>, and the band at 1595 cm<sup>-1</sup>, ascribable to the bending mode of neutral -NH<sub>2</sub> do not appear in the FT-IR spectrum of *zwitterionic* samples. Taken together these FT-IR observations reveal that MBG\_Sr2%\_SG\_Z and MBG\_Sr2%\_SD\_Z exhibits a mixed charged surface, due to the co-presence of NH<sub>3</sub><sup>+</sup> and COO<sup>-</sup> groups, respectively.

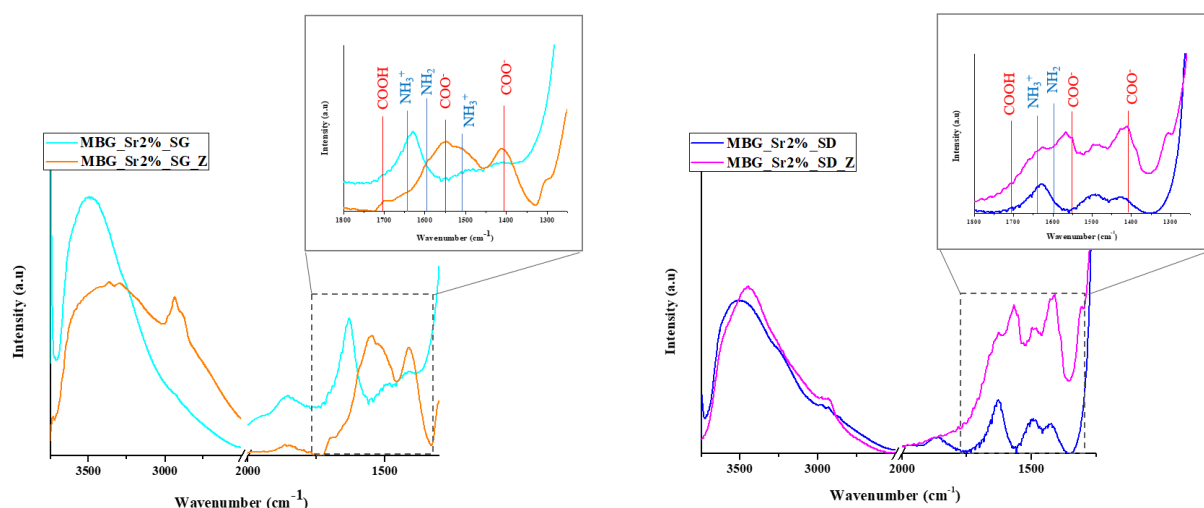


Fig. 4 FTIR spectra of MBG\_Sr2%\_SG and MBG\_Sr2%\_SD before and after *zwitterionization*.

Thermogravimetric analysis has been used to estimate the anchored organic components based on the weight loss. As reported in Fig SI 2, TG profiles of bare Sr-MBGs show solely a weight loss in the range 30-180°C, related to the elimination of the adsorbed water, revealing the absence of additional surface moieties. At variance, *zwitterionic* samples, two clear weight loss components were observed: the first below 200° C due to the release of the adsorbed



water, and a more significant step between 300 and 600°C, ascribable to the decomposition of anchored amino and carboxylate organic moieties.

Since these materials are intended for biomedical applications where the surface charge plays an essential role, their behaviour in aqueous media at different pH was investigated by  $\zeta$ -potential measurements, in order to determine the pH values at which the *zwitterionic* nature is preserved. As can be observed from the  $\zeta$ -potential vs. pH plots reported in Fig 5, unmodified Sr-MBGs exhibited negative  $\zeta$ -potential values within the whole pH range, due to the presence of deprotonated silanols ( $-\text{Si}-\text{O}^-$ ). These data are in good agreement with those reported in the literature, where the isoelectric point at around pH = 2 is reported for similar silica-based systems [43,44].

As already mentioned before,  $\zeta$ -potential analysis supported the optimisation of the functionalization protocol in term of organosilane initial ratio and reaction times. The first attempt conducted with an equimolar concentration of APST and CES, added simultaneously (MBG\_Sr2%\_Z\_1:1) led to the  $\zeta$ -potential value at pH 7.4 around -9 mV. This negative value can be ascribed both to a preferential grafting of CES with respect to APST or the presence of residual unreacted deprotonated silanols groups, leading to a larger population of negative charged ( $\text{COO}^-$  and  $\text{SiO}^-$ ), compared to protonated amino groups ( $-\text{NH}_3^+$ ).

A double concentration of APTS, followed by CES addition after 30 minutes of reaction (MBG\_Sr2%\_Z\_1:2), allowed to obtain less negative  $\zeta$ -potential value at pH 7.4 (-6 mV), thanks to a larger amount of amino groups grafted on the particle surface. Finally, a further increase of APTS concentration on equal addition time of CES led to a closer value of  $\zeta$ -potential to a global zero charge, given by the balance of positive and negative charges.  $\zeta$ -potential measurements of MBG\_Sr2%\_SG\_Z and MBG\_Sr2%\_SD\_Z (MBG\_Sr2%\_Z\_1:3) reveals positive values in the pH range 3-7, due to the protonation of amino groups ( $\text{NH}_2 > \text{NH}_3^+$ ), which reach a value close to zero ( $2.2 \pm 0.9$  mV and  $-2.8 \pm 1.2$  mV, respectively) at pH 7.4, which indicates the *zwitterionic* behaviour of both systems in physiological conditions.

Since MBG\_Sr2%\_SG\_Z and MBG\_Sr2%\_SD\_Z samples exhibited the required  $\text{NH}_3^+/-\text{COO}^-$  *zwitterionic* pairs and net surface charges close to zero at the physiological pH of 7.4, the biocompatibility and the capability to inhibit protein adhesion of these two functionalized samples have been tested and compared to the bare analogues.

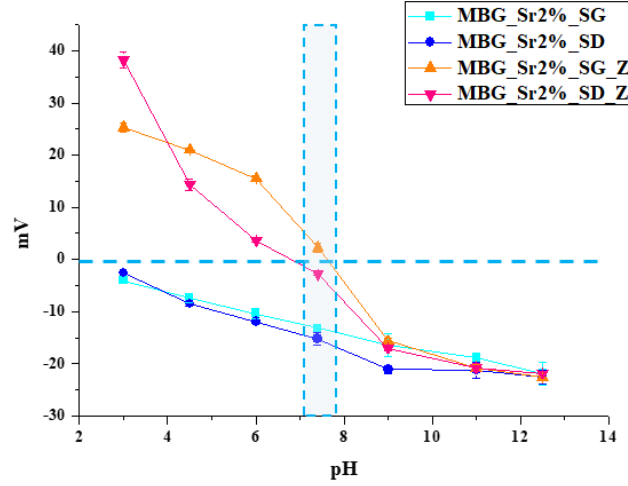


Fig. 5  $\zeta$ -potential measurements of MBG\_Sr2%\_SG and MBG\_Sr2%\_SD recorded at different pH before and after zwitterionization.

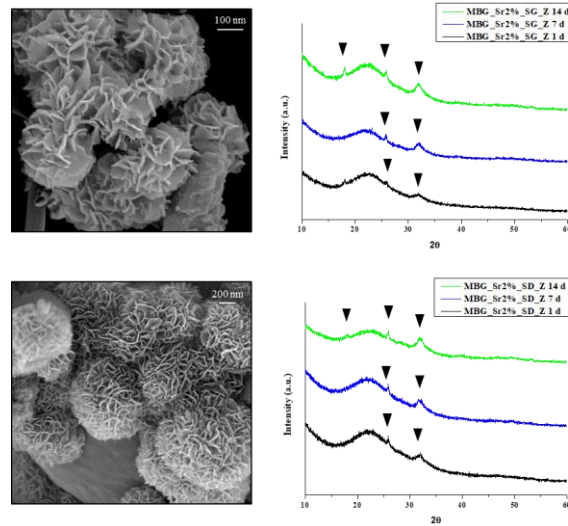


Fig. 6 FESEM images and XRD patterns of MBG\_Sr2%\_SG\_Z and MBG\_Sr2%\_SD\_Z after 1d, 7d and 14d of soaking in SBF (the most representative diffraction peaks of apatite phase are highlighted). The FESEM images are related to the surface after 14 days of incubation.

### 3.2. *In vitro* bioactivity of zwitterionic Sr-MBGs

After the grafting of APST and CES, both Sr-MBGs show a remarkable bioactive behaviour, retaining their ability to induce the deposition of the HA layer with fast kinetics [45]. In fact, after only 1 day of soaking, irrespective of the synthesis route, both Sr-MBGs appeared covered by a rough layer of globular agglomerates of apatite-like phase, that grew in size during the test, causing the final embedding of MBG particles overtime. As shown in Fig. 6, both particles after 7 days were fully covered by a compact layer of needle-like nanocrystals with the characteristic cauliflower morphology. EDS analysis performed on dried powders evidenced a Ca/P ratio of 1.7, typical value

reported in the literature for carbonated hydroxyapatite [46,47]. Furthermore, XRD patterns confirmed the formation of apatite-like layer with nanocrystalline nature (Fig 6), as revealed by peaks at 25.8 and 32.0  $2\theta$ , matching the HA reference (00-001-1008).

Finally, at each time point, the pH of the SBF solution was measured, resulting along the overall duration below 7.8, which allows osteoblasts to maintain their physiological activity[48].

The preservation of Sr-MBG bioactivity after *zwitterionization* was not fully predictable as the ion-exchange reactions which promote HA deposition could have been hampered or even fully blocked by the presence of the silane moieties. The assessment of this aspect was one the major goal of the work as it represents an essential feature for promoting bone regeneration.

### 3.3. $Sr^{2+}$ release from *zwitterionic* MBGs

The ion release of bare and functionalized samples was evaluated in Tris-HCl medium (pH 7.4); samples were incubated at 37 °C up to 14 days and, at selected time points (3 h, 1 day, 3 days, 7 days and 14 days), were centrifuged, aliquots were withdrawn and analysed by ICP-AES. As expected, the release properties of Sr-MBGs before functionalization resulted fully in agreement with those already reported by the authors in a previous contribution, confirming the fast ion diffusion inside the porous structure [16,19].

Strontium release from *zwitterionic* Sr-MBGs, evaluated in the same experimental conditions (Fig SI 3) revealed that samples after functionalization were able to release the total amount of incorporated  $Sr^{2+}$  ions with kinetics to those shown by the corresponding bare samples [16]. The final release  $Sr^{2+}$  concentration (1.6 ppm for MBG\_Sr2%\_SG\_Z and 4.4 ppm for MBG\_Sr2%\_SD\_Z) has the potential to stimulated osteogenic response as shown in several work, without inducing any cytotoxic effect [49]. In this regard [16], the authors recently demonstrated that the same concentration of  $Sr^{2+}$  was able to stimulate the expression of pro-osteogenic genes (COLL1A1, SPARC and OPG) of osteoblast-like cells cultured in the presence of only the dissolved ions released from Sr-substituted particles, confirming the key role exerted by strontium in stimulating osteoblast cell activity. Newly, the dissolution products released by Sr-containing bioactive glass nanoparticle were successfully proved to induce the stimulation of osteogenic response in hMSCs with the expression of genes associated to early-, mid- and late-osteogenic marker in the absence of osteogenic supplements [49].

### 3.4 Cell viability

The use of MBG nanocarriers for clinical applications requires excellent biocompatibility and absence of any cytotoxicity. In the literature, silica-based bioactive glass particles were widely proved to be biocompatible materials that exhibits low toxicity and lack of immunogenicity, degrading into nontoxic compounds (mainly silicic acid) in relatively short time periods[16,50–52].

Despite this lack of toxicity, the surface modification could provoke the appearance of toxicity due to several consequent aspects, among the other an enhanced uptake within the cells or the release of functional groups degradation products. To evaluate cytotoxicity, MC3T3-E1 preosteoblast cells were incubated with different amount of the both SD and SG before and after zwitterionization in cell culture medium. At determined incubation times (1, 2 and 5 days), cell viability was evaluated via the standard cell viability test by MTS reduction. The results showed that the tested particles, irrespective of their size and surface features, did not exhibit any cytotoxicity in preosteoblastic MC3T3-E1 (Fig 7) [53]. In order to further confirm these results lactate dehydrogenase (LDH) production were recorded after 1 day of cell incubation with the different Sr-MBG particles (before and after *zwitterionization*) at different concentrations. LDH is an enzyme released by cells in case of cell membrane rupture, thus indicating a cytotoxic effect. Interestingly, the results of LDH tests reported (Fig SI 4 A) obtained for MBG\_Sr2%\_SG and MBG\_Sr2%\_SD and the *zwitterionic* analogues, evidenced no cytotoxic effect up to the concentration of 75  $\mu\text{g/mL}$  and no significant differences were registered in comparison with the control test. These results were also confirmed by optical microscopy (Fig SI 4 B), where the cells adhered to the surface of the well appeared well spread without any apparent cell damage.

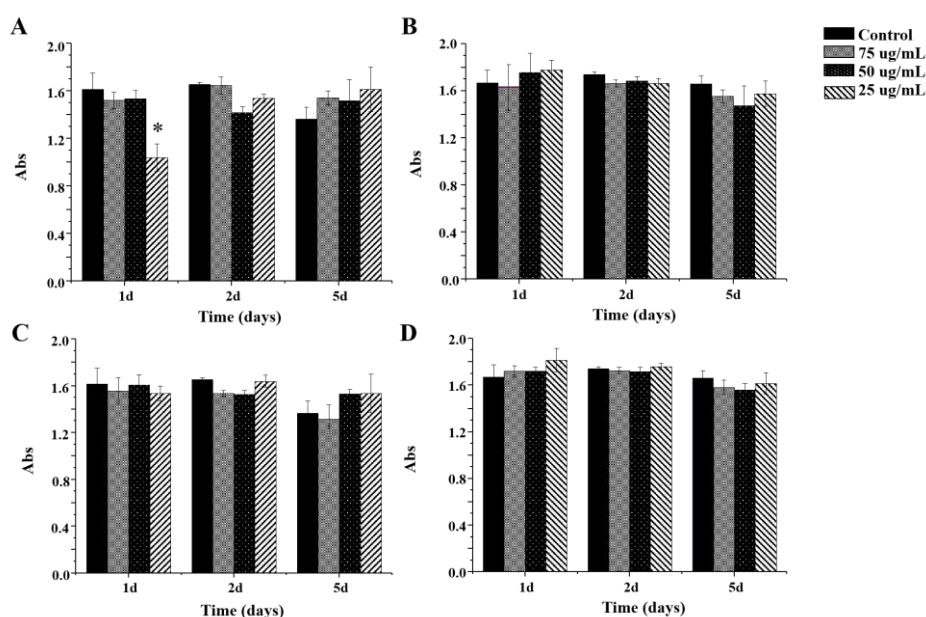


Fig. 7 Cell viability studies of the samples MBG\_Sr2%\_SG (A), MBG\_Sr2%\_SG\_Z (B), MBG\_Sr2%\_SD (C) and MBG\_Sr2%\_SD\_Z (D) at different concentration for MC3T3-E1 cell line and 1 d, 2 d and 5 d of exposure time. \*p <0.05 vs corresponding control without particles (ANOVA)

### 3.5 Mineralization assay

Differentiation is a process by which unspecialized cells, pre-osteoblasts, become specialized cells with the function to restore the bone. In this study, a preliminary experiment by monitoring the mineralization process in term of alizarin assay has been carried out to clarify if the *zwitterionization* process affect or not to the differentiation. Related results, reported in Fig 8 evidenced an increase of matrix mineralization for all Sr-substituted MBGs materials with respect to control, which is attributed to the osteogenic capability of released  $\text{Sr}^{2+}$  ions release as it has been previously reported [16,49,54]. After functionalization, no significant differences with respect to both pristine samples were observed, confirming that the *zwitterionization* process does not affect the alizarin production. These findings could be explained since the functionalized samples exhibit similar strontium release compared to the pristine samples, and consequently, also the associated osteogenic capability (in this case the mineralization).

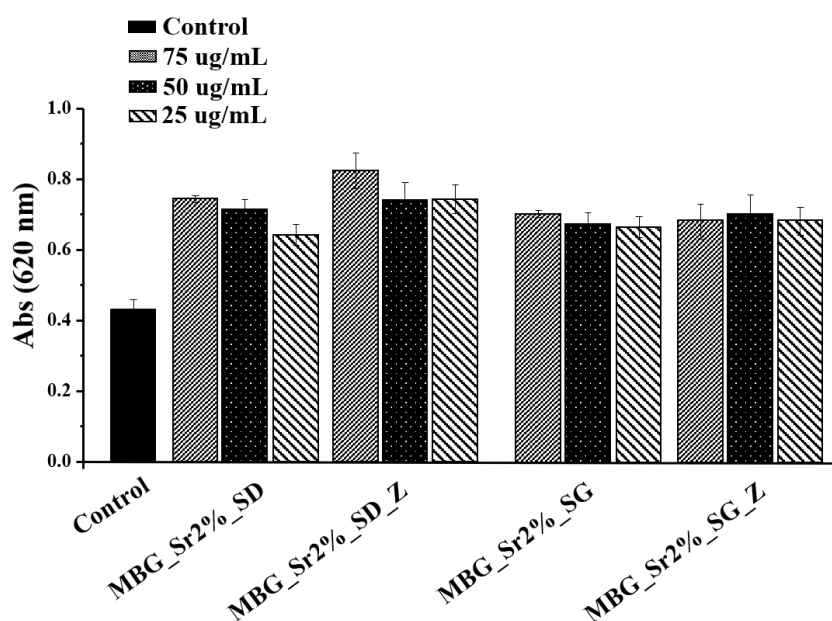


Fig. 8 Mineralization process in terms of alizarin assays of Sr-MBGs (SD and SG) before and after *zwitterionization* at different concentration (25, 50 and 75  $\mu\text{g/mL}$ ).

### 3.6 In vitro non-specific protein adhesion

Once demonstrated the *zwitterionic* nature and the biocompatibility of the functionalised Sr-MBG particles, their tendency to undergo nonspecific protein adsorption when soaked in biological fluids was evaluated by *in vitro* adsorption assays with two serum proteins, BSA and fibrinogen, respectively. Related results, displayed in Table 3,

show a notable decrease of protein adsorption for both proteins after *zwitterionization* process with a reduction of *c.a.* 85% and 86% of BSA and 70% and 54% of Fib for the MBG\_Sr2%\_SG\_Z and MBG\_Sr2%\_SD\_Z, respectively.

Table 3 Amount of BSA and fibrinogen adsorbed on the surfaces of Sr-MBGs before and after *zwitterionization* determined by SDS-PAGE technique.

| Sample        | BSA<br>(mg/g) | Fibrinogen<br>(mg/g) |
|---------------|---------------|----------------------|
| MBG_Sr2%_SG   | 348 ± 75      | 463 ± 79             |
| MBG_Sr2%_SG_Z | 51 ± 18       | 134 ± 58             |
| MBG_Sr2%_SD   | 170 ± 50      | 243 ± 58             |
| MBG_Sr2%_SD_Z | 24 ± 13       | 133 ± 57             |

This significant reduction is attributed to the presence of *zwitterionic* pairs, which are known to act as a barrier to non-specific protein adsorption [29,55] via a strongly adsorbed layer of water molecules solvating the charged terminal COO<sup>-</sup>/NH<sub>3</sub><sup>+</sup> groups via multiples hydrogen bounds.

After protein non-specific adsorption occurs, the Dh of the bare samples is expecting to increase, while the *zwitterionic* particle size will remain stable[55]. In fact, the hydrodynamic diameter of MBG\_Sr2%\_SG increased from 142 nm to 475 nm (Fig. SI 5), confirming the protein adsorption on the particle surface, due to an electrostatic interaction between the protein positive charges and the particle negative ones. On the other hands, the Dh of the MBG\_Sr2%\_SG\_Z remained stable after the incubation in the BSA solution (Fig. SI 5), confirming the anti-adhesive properties of the *zwitterionic* particles. This behaviour can be ascribe to the strong surface hydration layer formed by the neutral *zwitterionic* structure[55].

The obtained data reveal a significant larger reduction in protein adhesion for MBG\_Sr2%\_SG\_Z compared MBG\_Sr2%\_SD\_Z, when both compared to their corresponding bare samples, that can be attributed to the drastic decrease of surface area upon functionalization evidenced by nitrogen adsorption-desorption analysis (Table 2) for Sr-MBG prepared by SG approach.

#### 4. Conclusions

On the basis of the previously reported preparative procedures [16,17], in this study, promising advanced biomaterials based on strontium-releasing mesoporous bioactive glasses were boosted up with an anti-adhesive *zwitterionic* surface with the aim of promoting bone regeneration and simultaneously inhibiting non-specific biomolecule adsorption and, consequently, bacterial adhesion. To reach this goal, Sr-MBGs have been produced in the form of

nano- and micro-particles and, subsequently, modified by co-grafting a hydrolysable short chain silane bearing an amino (aminopropyl silanetriol, APST) and a carboxylic (carboxyethylsilanetriol, CES), respectively. Compared to other approaches which involved several synthetic steps and different intermediate products [31], a straightforward and clean procedure was optimized by modulating the relative amount of APST and CES and their reaction time, to provide Sr-MBG surface with an overall electrical neutrality under physiological conditions (pH=7.4).

The modification of the surface with *zwitterionic* pairs proved not to alter the ability to release strontium ions within concentrations which are able to promote early osteogenic differentiation [16] and mineralized matrix deposition. Furthermore, no cytotoxic effect was demonstrated by the cell culture with MC3T3-E1 preosteoblast cells.

*In vitro* non-specific protein adhesion assay demonstrated that the successful grafting of the *zwitterionic* pairs onto Sr-MBG surfaces reduced BSA and Fib adhesion up to *ca.* 85% and 70%, respectively. The excellent results obtained by the protein adhesion assay could pave the way to further investigations, in order to demonstrate the anti-adhesive properties of the material also against bacteria attachment.

## 5. Acknowledgements

This work was supported by Compagnia di San Paolo under the initiative “Metti in rete la tua idea di ricerca”. M.V.R. and I.I.B. acknowledge funding from the European Research Council (Advanced Grant VERDI; ERC-2015-AdG Proposal No. 694160).

## 6. References

- [1] T. Winkler, F.A. Sass, G.N. Duda, K. Schmidt-bleek, A review of biomaterials in bone defect healing , remaining shortcomings and future opportunities for bone tissue engineering, *Bone Joint Res* 7 (2018) 232–243.
- [2] N.P. Haas, Callusmodulation Fiktion oder Realität?, (2000) 987–988.
- [3] C. Schlundt, C.H. Bucher, S. Tsitsilonis, H. Schell, G.N. Duda, K. Schmidt-bleek, Clinical and Research Approaches to Treat Non-union Fracture, *Current Osteoporosis Reports* (2018) 155–168.
- [4] D. Campoccia, L. Montanaro, C. Renata, Biomaterials A review of the biomaterials technologies for infection-resistant surfaces, *Biomaterials*. 34 (2013) 8533–8554. doi:10.1016/j.biomaterials.2013.07.089.
- [5] I. Izquierdo-Barba, M. Colilla, M. Vallet-Regí, Zwitterionic ceramics for biomedical applications, *Acta Biomater.* 40 (2016) 201–211. doi:10.1016/j.actbio.2016.02.027.

- [6] S. Sánchez-Salcedo, M. Colilla, I. Izquierdo-Barba, M. Vallet-Regí, Design and preparation of biocompatible zwitterionic hydroxyapatite, *J. Mater. Chem. B.* (2013) 1595–1606. doi:10.1039/C3TB00122A.
- [7] J.. Mader, M.E. Shirtliff, S.C. Bergquist, J. Calhoun, Antimicrobial Treatment of Chronic Osteomyelitis, *Clin. Orthop. Relat. Res.* (1999) 47–65.
- [8] R.O. Darouiche, Treatment of Infections Associated with Surgical Implants, *N. Engl. J. Med.* 350 (2004) 1422-1429.
- [9] R. Haidar, A. Der Boghossian, B. Atiyeh, Duration of post-surgical antibiotics in chronic osteomyelitis : empiric or evidence-based?, *Int. J. Infect. Dis.* 14 (2020) e752–e758. doi:10.1016/j.ijid.2010.01.005.
- [10] J.D. Whitehouse, N.D. Friedman, K.B. Kirkland, W.J. Richardson, D.J. Sexton, The impact of surgical-site infections following orthopedic surgery at a community hospital and a university hospital: adverse quality of life, excess length of stay, and extra cost, *Infect. Control Hosp. Epidemiol.* 23 (2012) 183–189.
- [11] J.W. Costerton, P.S. Stewart, E.P. Greenberg, Bacterial Biofilms : A Common Cause of Persistent Infections, *Science* 284 (1999) 1318–1323.
- [12] R. García-Alvarez, I. Izquierdo-Barba, M. Vallet-Regí, 3D scaffold with effective multidrug sequential release against bacteria biofilm, *Acta Biomater.* 49 (2017) 113–126.
- [13] R.M. Donlan, J.W. Costerton, Biofilms : Survival Mechanisms of Clinically Relevant Microorganisms, *Clin. Microbiol. Rev.* 15 (2002) 167–193.
- [14] J.W. Costerton, L. Montanaro, C.R. Arciola, Biofilm in Implant Infections: Its Production and Regulation, *Int. J. Artif. Organs.* 28 (2005) 1062–1068.
- [15] D. Campoccia, F. Testoni, S. Ravaoli, I. Cangini, A. Maso, P. Speziale, L. Montanaro, L. Visai, C.R. Arciola, Orthopedic implant infections : Incompetence of *Staphylococcus epidermidis* , *Staphylococcus lugdunensis* , and *Enterococcus faecalis* to invade osteoblasts, *J. Biomed. Mater. Res* 104 (2015) 788–801.
- [16] S. Fiorilli, G. Molino, C. Pontremoli, G. Iviglia, E. Torre, C. Cassinelli, M. Morra, C. Vitale-Brovarone, The incorporation of strontium to improve bone-regeneration ability of mesoporous bioactive glasses, *Materials* 11 (2018) 678.
- [17] A. Bari, G. Molino, S. Fiorilli, C. Vitale-brovarone, Novel multifunctional strontium-copper co-substituted mesoporous bioactive particles, *Mater. Lett.* 223 (2018) 37–40.



- [18] M. Shi, Z. Chen, S. Farnaghi, T. Friis, X. Mao, Y. Xiao, C. Wu, Copper-doped mesoporous silica nanospheres, a promising immunomodulatory agent for inducing osteogenesis, *Acta Biomater.* 30 (2016) 334–344.
- [19] C. Pontremoli, M. Boffito, S. Fiorilli, R. Laurano, A. Torchio, A. Bari, C. Tonda-Turo, G. Ciardelli, C. Vitale-Brovarone, Hybrid injectable platforms for the in situ delivery of therapeutic ions from mesoporous glasses, *Chem. Eng. J.* 340 (2018) 103–113.
- [20] S. Lin, J.R. Jones, The effect of serum proteins on apatite growth for 45S5 Bioglass and common sol-gel derived glass in SBF, *Biomed. Glasses* 4 (2018) 13–20.
- [21] C. Blaszykowski, S. Sheikh, M. Thompson, Surface chemistry to minimize fouling from blood-based fluids, *Chem. Soc. Rev.* 41 (2012) 5599–5612.
- [22] H. Zhang, M. Chiao, Anti-fouling coatings of poly(dimethylsiloxane) devices for biological and biomedical applications, *J. Med. Biol. Eng.* 35 (2015) 143–155.
- [23] E.P. Magennis, A.L. Hook, M.C. Davies, C. Alexander, P. Williams, M.R. Alexander, Engineering serendipity: High-throughput discovery of materials that resist bacterial attachment, *Acta Biomater.* 34 (2016) 84–92.
- [24] W.H. Kuo, M.J. Wang, H.W. Chien, T.C. Wei, C. Lee, W.B. Tsai, Surface modification with poly(sulfobetaine methacrylate-co-acrylic acid) to reduce fibrinogen adsorption, platelet adhesion, and plasma coagulation, *Biomacromolecules* 12 (2011) 4348–4356.
- [25] A.J. Keefe, N.D. Brault, S. Jiang, Suppressing surface reconstruction of superhydrophobic PDMS using a superhydrophilic zwitterionic polymer, *Biomacromolecules* 13 (2012) 1683–1687.
- [26] S. Chen, L. Li, C. Zhao, J. Zheng, Surface hydration : Principles and applications toward low-fouling / nonfouling biomaterials, *Polymer* 51 (2010) 5283–5293.
- [27] K. Ishihara, Y. Iwasaki, Reduced protein adsorption on novel phospholipid polymers, *J. Biomater. Appl.* 13 (1998) 111–127.
- [28] K. Ishihara, H. Nomura, T. Mihara, K. Kurita, Y. Iwasaki, N. Nakabayashi, Why do phospholipid polymers reduce protein adsorption?, *J. Biomed. Mater. Res.* 39 (1998) 323–330.
- [29] R. Jin, Z. Liu, Y. Bai, Y. Zhou, X. Chen, Multiple-Responsive Mesoporous Silica Nanoparticles for Highly Accurate Drugs Delivery to Tumor Cells, *ACS omega*, 3 (2018), 4306–4315.

- [30] N. Encinas, M. Angulo, C. Astorga, I. Izquierdo-barba, M. Vallet-regí, *Acta Biomaterialia* Mixed-charge pseudo- zwitterionic mesoporous silica nanoparticles with low-fouling and reduced cell uptake properties, 84 (2019) 317–327.
- [31] S. Sánchez-Salcedo, A. García, M. Vallet-regí, Prevention of bacterial adhesion to zwitterionic biocompatible mesoporous glasses, *Acta Biomater.* 57 (2017) 472–486.
- [32] L. Pontiroli, M. Dadkhah, G. Novajra, I. Tcacencu, S. Fiorilli, C. Vitale-Brovarone, An aerosol-spray-assisted approach to produce mesoporous bioactive glass microspheres under mild acidic aqueous conditions, *Mater. Lett.* 190 (2017) 111–114.
- [33] L.T. Zhuravlev, Surface characterization of amorphous silica-a review of work from the former USSR, *Colloids Surfaces A Physicochem. Eng. Asp.* 74 (1993) 71–90.
- [34] R.J. Hunter, Interaction between Colloidal Particles, *Zeta Potential Colloid Sci.* (1981) 363-369.
- [35] A.L.B. Maçon, T.B. Kim, E.M. Valliant, K. Goetschius, R.K. Brow, D.E. Day, A. Hoppe, A.R. Boccaccini, I.Y. Kim, C. Ohtsuki, T. Kokubo, A. Osaka, M. Vallet-Regí, D. Arcos, L. Fraile, A.J. Salinas, A. V. Teixeira, Y. Vueva, R.M. Almeida, M. Miola, C. Vitale-Brovarone, E. Vernè, W. Höland, J.R. Jones, A unified in vitro evaluation for apatite-forming ability of bioactive glasses and their variants, *J. Mater. Sci. Mater. Med.* 26 (2015) 115-125.
- [36] K.K. Kaysinger, W.K. Ramp, Interaction between Colloidal Particles, in: *Zeta Potential Colloid Sci.*, (1981) 363–369.
- [37] D. Lozano, M. Manzano, J.C. Doadrio, A.J. Salinas, M. Vallet-Regí, E. Gómez-Barrena, P. Esbrit, Osteostatin-loaded bioceramics stimulate osteoblastic growth and differentiation, *Acta Biomater.* 6 (2010) 797–803.
- [38] N. Gomez-Cerezo, ab D.A. and M.V.-R. I. Izquierdo-Barba, Tailoring the biological response of mesoporous bioactive materials, *J. Mater. Chem. B* (2015) 3810–3819.
- [39] M. Guembe, I. Izquierdo-Barba, B. González, M. Vallet-Regí, J. Díez, M. Colilla, D. Pedraza, Mesoporous silica nanoparticles decorated with polycationic dendrimers for infection treatment, *Acta Biomater.* 68 (2018) 261–271.
- [40] F. Hoffmann, M. Cornelius, J. Morell, M. Fröba, Silica-based mesoporous organic-inorganic hybrid

materials, *Angew. Chemie - Int. Ed.* 45 (2006) 3216–3251.

- [41] S. Fiorilli, B. Onida, B. Bonelli, E. Garrone, In situ infrared study of SBA-15 functionalized with carboxylic groups incorporated by a Co-condensation route, *J. Phys. Chem. B.* 109 (2005) 16725–16729.
- [42] S. Fiorilli, L. Rivoira, G. Calì, M. Appendini, M.C. Bruzzoniti, M. Coisson, B. Onida, Iron oxide inside SBA-15 modified with amino groups as reusable adsorbent for highly efficient removal of glyphosate from water, *Appl. Surf. Sci.* 411 (2017) 457–465.
- [43] L. Dalstein, E. Potapova, E. Tyrode, The elusive silica/water interface: Isolated silanols under water as revealed by vibrational sum frequency spectroscopy, *Phys. Chem. Chem. Phys.* 19 (2017) 10343–10349.
- [44] R.K. Iler, I.R. K, The Chemistry of Silica: Solubility, Polymerization, Colloid and Surface Properties and Biochemistry of Silica, *Sci. Geol.*, 35 (1979) 93–94.
- [45] I. Izquierdo-Barba, M. Vallet-Regí, Mesoporous bioactive glasses: Relevance of their porous structure compared to that of classical bioglasses, *Biomed. Glas.* 1 (2015) 140–150.
- [46] V. Uskoković, D.P. Uskoković, Nanosized hydroxyapatite and other calcium phosphates: Chemistry of formation and application as drug and gene delivery agents, *J. Biomed. Mater. Res. - Part B Appl. Biomater.* 96 B (2011) 152–191.
- [47] K. Lin, C. Wu, J. Chang, Advances in synthesis of calcium phosphate crystals with controlled size and shape, *Acta Biomater.* 10 (2014) 4071–4102.
- [48] K.K. Kaysinger, W.K. Ramp, Extracellular pH modulates the activity of cultured human osteoblasts, *J. Cell. Biochem.* 1 (1998) 83–89.
- [49] P. Naruphontjirakul, O. Tsigkou, S. Li, A.E. Porter, J.R. Jones, Human mesenchymal stem cells differentiate into an osteogenic lineage in presence of strontium containing bioactive glass nanoparticles, *Acta Biomater.* 90 (2019) 373–392.
- [50] J. Lu, M. Liong, Z. Li, J.I. Zink, F. Tamanoi, Biocompatibility, biodistribution, and drug-delivery efficiency of mesoporous silica nanoparticles for cancer therapy in animals, *Small.* 6 (2010) 1794–1805.
- [51] T.H. Qazi, S. Hafeez, J. Schmidt, G.N. Duda, A.R. Boccaccini, E. Lippens, Comparison of the effects of 45S5 and 1393 bioactive glass microparticles on hMSC behavior, *J. Biomed. Mater. Res. A* 105 (2017) 2772–2782.
- [52] P. Naruphontjirakul, A.E. Porter, J.R. Jones, In vitro osteogenesis by intracellular uptake of strontium

containing bioactive glass nanoparticles, *Acta Biomater.* 66 (2018) 67–80.

- [53] I. Izquierdo-Barba, S. Sánchez-Salcedo, M. Colilla, M.J. Feito, C. Ramírez-Santillán, M.T. Portolés, M. Vallet-Regí, Inhibition of bacterial adhesion on biocompatible zwitterionic SBA-15 mesoporous materials, *Acta Biomater.* 7 (2011) 2977–2985.
- [54] J. Zhang, S. Zhao, Y. Zhu, Y. Huang, M. Zhu, C. Tao, C. Zhang, Three-dimensional printing of strontium-containing mesoporous bioactive glass scaffolds for bone regeneration, *Acta Biomater.* 10 (2014) 2269–2281.
- [55] S. Sanchez-salcedo, M. Vallet-regí, S. Allaf, C.A. Glackin, I. Zink, Mesoporous core-shell silica nanoparticles with anti-fouling properties for ovarian cancer therapy, *Chemical Engineering Journal* 340 (2018) 114–124.